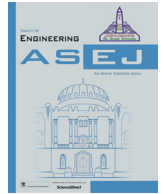




Contents lists available at ScienceDirect

Ain Shams Engineering Journal

journal homepage: www.sciencedirect.com



Electrical Engineering

# Dynamic reluctance air gap modeling and experimental evaluation of electromagnetic characteristics of five-phase permanent magnet synchronous generator for wind power application

Raja Ram Kumar, S.K. Singh, R.K. Srivastava, R.K. Saket \*

Indian Institute of Technology (Banaras Hindu University), Varanasi, UP, India

## ARTICLE INFO

## Article history:

Received 2 June 2018

Revised 16 September 2019

Accepted 18 September 2019

Available online xxx

## Keywords:

Wind power

Five phase

Permanent magnet synchronous generator

Dynamic reluctance network modeling

Finite element method

## ABSTRACT

This paper presents the design and analysis of electromagnetic characteristics of a five phase permanent magnet synchronous generator for direct drive wind energy conversion system (WECS). In this study, simple and accurate Dynamic Reluctance Network Modeling is used for design and optimization of generator. The anisotropic structure of stator and rotor for the accurate prediction of flux distribution in the air gap and electromagnetic performance is accounted by the dynamic variation of air gap reluctance in an electrical period. This model considers the leakage flux paths for machine design optimization to achieve better performance. In this context, three permanent magnet (PM) materials namely NdFeB, SmCo and ferrite are considered to evaluate the generated voltage. The dimensions of these permanent magnets are varied and performance under normal and saturated core condition is evaluated. A prototype is developed in the machine laboratory of the IIT(BHU) Varanasi (India) and results obtained in accordance with Finite Element Method.

© 2019 Ain Shams University. Production and hosting by Elsevier B.V. This is an open access article under the CC BY-NC-ND license (<http://creativecommons.org/licenses/by-nc-nd/4.0/>).

## 1. Introduction

Due to environmental issues, renewable energy has become the current trend of energy generation [1]. Energy sources such as solar, wind, biomass, geothermal, etc are quite popular since they are locally available but are indefinite source of energy. Wind power is a sustainable energy source that yields cheaper energy production [2,3]. To harness maximum amount of energy from wind for variable speed, a suitable generating system is required. Permanent magnet synchronous generator (PMSG) is most suited for this purpose since it is a direct drive system and generates voltage for wide range of speeds, whereas conventional generators operate at a single fixed speed and have issues of frequent gear box and slip ring maintenance [4]. PMSG possesses advantages like

high efficiency [5], high power density, light weight and ease of use as compared to conventional systems [6,7]. The power density can be further improved by using multi-phase systems. Multi-phase generators possess fault tolerance capability since they can operate stably even when more than one phase is under fault, with acceptable output [8]. It has inherent features of minimizing the space harmonics, torque ripples and suppressing the vibrations, due to which it is fit for direct drive wind power applications [9,10]. With optimized design the torque ripple and harmonics in the generated voltage could be further reduced.

To design and analyse a generator, mainly two techniques are reported, analytical and finite element analysis. In Finite Element Method (FEM), for the calculation of electromagnetic field distribution, the geometry has to be discretized and thus the solution become more complex, time consuming but at the same time accuracy improves [11]. Analytical models are important tools for design, analysis and optimization of electrical machines because; these are very quick in computing the electromagnetic field solutions. In [12,13] authors have reported an analytical model and computed the performance of PM machines based on sub domain modeling technique but it requires enough information about boundary conditions and mathematical calculations are rigorous. Reluctance network modeling technique is very popular owing to its simplicity, fast and accurate prediction of performance for all

\* Corresponding author.

E-mail addresses: [rajaram.rs.eee@iitbhu.ac.in](mailto:rajaram.rs.eee@iitbhu.ac.in) (R.R. Kumar), [sksingh.eee@iitbhu.ac.in](mailto:sksingh.eee@iitbhu.ac.in) (S.K. Singh), [rksrivastava.eee@iitbhu.ac.in](mailto:rksrivastava.eee@iitbhu.ac.in) (R.K. Srivastava), [rksaket.eee@iitbhu.ac.in](mailto:rksaket.eee@iitbhu.ac.in) (R.K. Saket).

Peer review under responsibility of Ain Shams University.



<https://doi.org/10.1016/j.asej.2019.09.004>

2090-4479/© 2019 Ain Shams University. Production and hosting by Elsevier B.V.

This is an open access article under the CC BY-NC-ND license (<http://creativecommons.org/licenses/by-nc-nd/4.0/>).

Please cite this article as: R. R. Kumar, S. K. Singh, R. K. Srivastava et al., Dynamic reluctance air gap modeling and experimental evaluation of electromagnetic characteristics of five-phase permanent magnet synchronous generator for wind power application, Ain Shams Engineering Journal, <https://doi.org/10.1016/j.asej.2019.09.004>

## Nomenclature

### List of symbols

$l_m$	length of magnet
$L$	core length of generator
$L_i$	iron core length
$\mu_{fe}$	relative permeability of iron
$\mu_o$	$4\pi \times 10^{-7}$
$H_{pm}$	height of magnets
$H_c$	coercivity of PM

$N_c$	no. of turns per coil
$I_{a,b,c,d,e}$	phase current
$g$	airgap length
$g_{eff}$	effective airgap length
$N_{ph}$	number of turns per phase
$f$	frequency
$\Theta_{er}$	rotor rotation electrical angle
$\beta$	angular length of magnet

kind of machines. In this context, machine is represented by lumped parameter reluctance network and reluctance of air gap is modelled considering the effective air gap length using the carter coefficient. This accounts for the slotting effect of machine for the performance evaluation [14]. The leakage flux affects the performance and the analysis is effectively evaluated [15] in terms of flux density distribution. Today, researchers are working on variable air gap reluctance network which implies reluctance of air gap varies with variation in the position of rotor which in turn provides actual variation of presence of the air gap. This accounts for actual distribution of flux in the air gap. For computation of interaction between stator teeth and PMs, many techniques have been proposed [16].

Although, many literatures incorporated the effects of saturation, slotting and armature reaction with some assumptions to avoid the complexity in the machine reluctance network model due to which they compromise with the accuracy of electromagnetic performance results. The improvement of model accuracy, evaluation of power density of the optimized design and performance studies under saturation condition are most motivating factors for the authors. This paper focuses on design and the evaluation of electromagnetic performance of the five phase permanent magnet synchronous generator (FP-PMSG) for direct-drive wind power applications. Basically, it is highlighted to the dynamic reluctance network modelling for model accuracy, adverse effect of core saturation on the performance, power density and electromagnetic performance of FP-PMSG. The prediction of performances is evaluated using dynamic reluctance network modeling (DRNM). This network comprises linear, non-linear and dynamic reluctances together with flux sources. Armature winding and permanent magnets are two flux sources whose Flux amplitude varies with current density, material properties and dimensional parameters. In this paper, authors have taken three different PM materials namely ferrite, SmCo and NdFeB to evaluate their effect on the performance of generator, where the focus would be on air gap reluctance. The air gap reluctance varies with rotor position while core reluctance varies with saturation of magnetic core material. The saturation of core leads to adverse effect on generated voltage. To get the optimal performance, the leakage flux reluctance is also considered in the dynamic reluctance network. To validate the calculated results using DRNM, Finite element analysis is performed and results are found in good agreement. Furthermore, a prototype is fabricated for the experimental validation of the predicted and simulated results.

This Paper is organized in the following manners. The Section 2 of this manuscript introduces the proposed topology, winding details, voltage developed and design details. The Section 3 elaborates the dynamic reluctance network modeling for the proposed generator and integrates the effect of rotor rotation within the model. The Section 4 of the paper describes the experimental set-up along with results. The comparisons of predicted, FEM and experimental results are discussed in Section 5. Finally, Section 6 summarises the concluding remarks.

## 2. Proposed topology and machine description

The proposed topology of the five phases PMSG, consisting of stator and rotor with 8 poles is shown in Fig. 1 and Fig. 2.

There are 8 permanent magnets mounted on the surface of rotor. Magnetic poles are having  $36^\circ$  arc-span and 2.5 mm thickness. Stator is having 60 slots consisting of double layer fractional slot winding of five phases and 8 poles. Each phase of the winding is mutually  $72^\circ$  phase apart. It consists of 240 turns placed in 12 coils. Which are short-pitched by  $12^\circ$ . The winding connection details for phase A is presented in Table 1. The voltage developed in each of the 12 coils ( $C_a, C_b, C_c, C_d, C_e, C_f, C_g, C_h, C_i, C_j, C_k$  and  $C_l$ ) with rotor position is shown in Fig. 3. The phasor sum of all these coil voltages is shown in Fig. 4. The specification and dimensional details of the generator are given in Table 2 and Table 3, respectively.

## 3. Dynamic reluctance network model

To predict the flux distribution and electromagnetic performance of the generator, a dynamic reluctance network model is adopted. DRNM comprises linear, non-linear and variable reluctances together with Magneto-Motive Force (MMF) sources which are shown in Fig. 5.

In this model, permanent magnet and five-phase armature windings are the main sources of flux. The armature winding flux

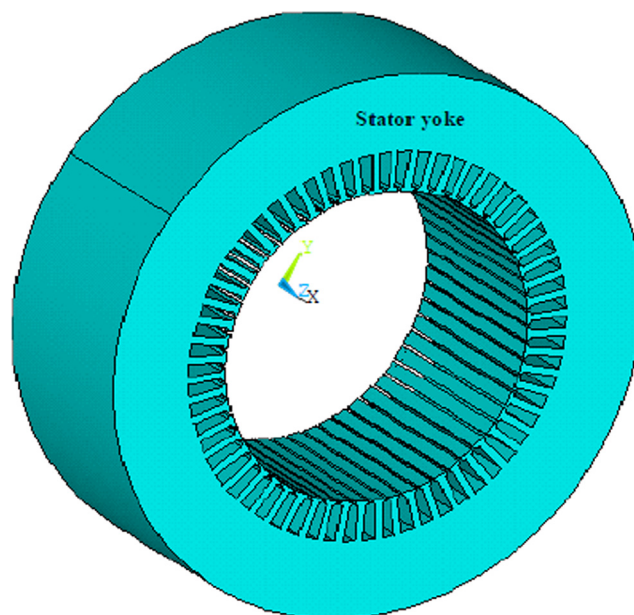


Fig. 1. Stator.

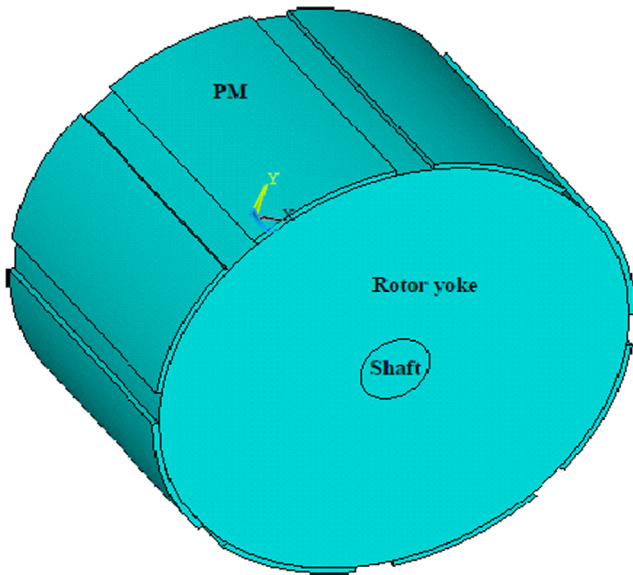


Fig. 2. Rotor.

depends upon the current density, whereas the magnet flux is decided by the magnetic material and its dimensional parameters. The variable reluctance in the model is corresponds to air gap reluctance. The reluctance of air gap varies with rotor position and interaction of PM with stator teeth, as demonstrated in DRNM. Non-linear reluctances are stator and rotor core reluctances originating due to saturation of ferromagnetic material. Stator teeth are the most sensitive part with respect to saturation. Due to saturation, the permeability of core starts to decrease which derates the machine performance. Linear reluctances are stator tooth tip to tip, permanent magnet reluctance and their leakage flux path reluctance in model. Fig. 6 represent the one-fourth linear model of generator in which three fluxes are shown, one for the main and other two for the leakage fluxes. Main flux traverses through PM-air-stator core-rotor core whereas leakage flux travels from magnet-air-rotor iron, and magnet-air-magnet.

DRNM only shows one fourth model because of its quarter symmetry. It consists of 34 nodes, 79 branches and 46 loops corresponding to  $t = 0$  sec. The linear reluctance is calculated using Eq. (1) and non-linear reluctances of different sections are calculated using Eq. (2). There are 15 stator slots having an upper and lower layer of winding in the model. This winding shows mmf sources which are present in the model with tooth reluctance. These mmf sources are computed from the phase currents using Eq. (3), where  $N_c$  is the number of turns per coil. The air gap reluctance is not easy to calculate because it changes dynamically as rotor rotates. It is based on the interaction of PMs and stator tooth. There are 15 reluctances with one PM interaction in the reluctance network and all reluctances can be computed using Eq. (4). The PMs are the main MMF sources in this network and can be computed with Eq. (5). The leakage reluctances of magnet to magnet and magnet to rotor iron can be computed using the circular arc-straight technique. A detailed description of this method is explained in Sections 3.1 and 3.2 respectively. The flux in each part of the model can be found using Eq. (6). Eq. (7) represents the reluctance matrix corresponding to the model.

Linear reluctance ( $R_l$ )

$$R_l = \frac{l_l}{\mu_0 \mu_r A_l} \tag{1}$$

where  $l_l$  is the length of segment in which flux flows,  $A_l$  is the corresponding area of the flux tube,  $\mu_r$  is the relative permeability of the material.

Non-linear reluctance ( $R_{nl}$ )

$$R_{nl} = \frac{l_{nl}}{\mu_0 \mu_{feB_{nl}} A_{nl}} \tag{2}$$

where  $l_{nl}$  is the length of segment in which flux flows,  $A_{nl}$  is the corresponding area of the flux tube,  $\mu_{fe B_{nl}}$  is permeability function dependent upon the flux density in the material.

MMF sources connected in the stator tooth due to winding

$$MMF_w = [f_1 \ f_2 \ f_3 \dots f_{15}]^T = N_c \cdot \begin{pmatrix} 2 & 0 & 0 & 0 & 0 \\ 0 & 0 & 0 & -2 & 0 \\ 0 & 1 & 0 & -1 & 0 \\ 0 & 2 & 0 & 0 & 0 \\ 0 & 0 & 0 & 0 & -2 \\ 0 & 0 & 1 & 0 & -1 \\ 0 & 0 & 2 & 0 & 0 \\ -2 & 0 & 0 & 0 & 0 \\ -1 & 0 & 0 & 1 & 0 \\ 0 & 0 & 0 & 2 & 0 \\ 0 & -2 & 0 & 0 & 0 \\ 0 & -1 & 0 & 0 & 1 \\ 0 & 0 & 0 & 0 & 2 \\ 0 & 0 & -2 & 0 & 0 \\ 1 & 0 & -1 & 0 & 0 \end{pmatrix} \cdot \begin{pmatrix} I_a \\ I_b \\ I_c \\ I_d \\ I_e \end{pmatrix} \tag{3}$$

where  $f_1, f_2, f_3, \dots, f_{15}$  are the  $MMF_w$  sources connected corresponding to stator tooth branch.

Reluctance of air gap ( $R_{gi}$ ) due to interaction of PM with  $i^{th}$  stator tooth

$$R_{gi} = \frac{g}{\mu_0 \cdot \text{width} \cdot L} \tag{4}$$

where  $\text{width} = r_g \cdot \theta_{t-pm}$  and  $\theta_{t-pm}$  is the interaction angle between tooth and PM and  $r_g$  is the radius of air gap.

MMF due to PM

$$MMF_{pm} = H_c \cdot H_{pm} \tag{5}$$

where  $H_c$  is the coercivity and  $H_{pm}$  is the height of PM in the direction of magnetization.

The RN method results in a set of linear equations which should be solved to obtain magnetic fluxes.

$$[\phi] = [R]^{-1} [MMF] \tag{6}$$

$$[R] = \begin{pmatrix} R_{1,1} & \dots & R_{1,46} \\ \vdots & \ddots & \vdots \\ R_{46,1} & \dots & R_{46,46} \end{pmatrix} \tag{7}$$

Table 1  
Winding connection for phase A.

Coil	1	8	9	16	23	24	31	38	39	46	53	54
In	1	15	16	16	30	31	31	45	46	46	60	1
Out	8	8	9	23	23	24	38	38	39	53	53	54

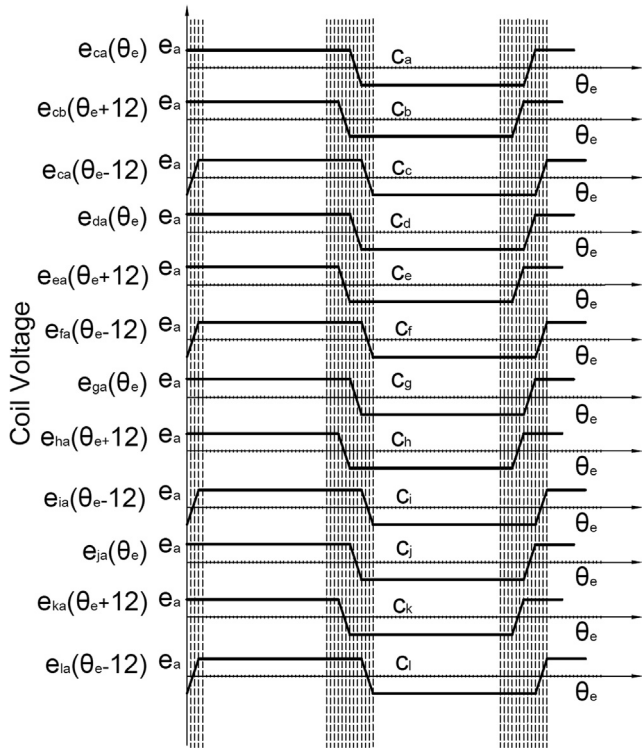


Fig. 3. Coil voltage.

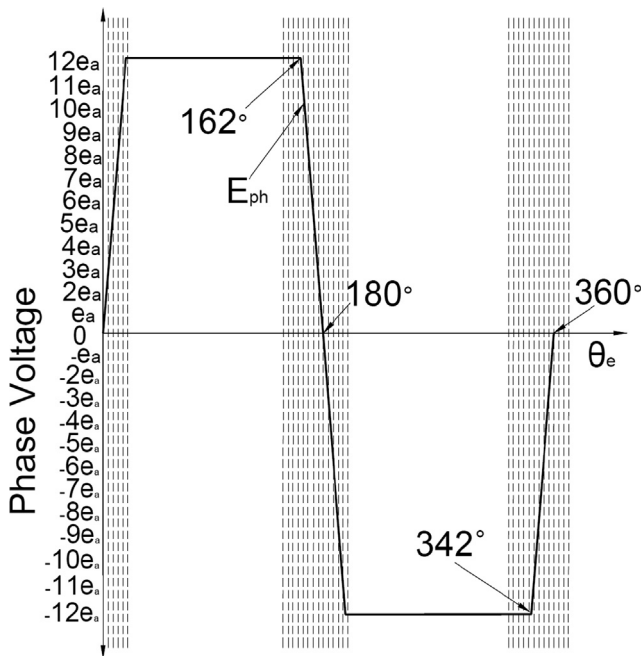


Fig. 4. Phase voltage.

Table 2  
Rating of machine.

Parameter	Value
Power	3.42 kVA
stator per phase voltage	171.0 V
phase current	4 A
Number of phases	5
Speed	400 rpm

Table 3  
Design parameters.

Design parameter	Value
Shaft radius	20 mm
Rotor outer radius	95 mm
Height of magnet	2.5 mm
Air gap length	2.3 mm
width of sleeve	0.2 mm
Inner radius of stator	100 mm
Outer radius of stator	175 mm
Area of slot	123.27 mm <sup>2</sup>

where R is (46 × 46), MMF is (46 × 1) and the flux is (46 × 1) matrix corresponding to model.

### 3.1. Reluctance calculation for magnet to magnet leakage path

The leakage reluctance of magnet to magnet flux path can be computed using circular arc-straight technique for considering the flux accurately [17]. The leakage paths reluctance is calculated on the basis of their dimensional details and material properties using Eq. (9). Fig. 7 shows the path of leakage flux between magnets to magnets.

Permeance of magnet to magnet leakage flux path ( $P_{mm}$ )

$$P_{mm} = \int_0^{g_{eff}} \frac{\mu_0 L}{\delta + \pi \zeta} d\zeta = \frac{1}{R_{mm}} \quad (8)$$

Reluctance of magnet to magnet leakage flux path ( $R_{mm}$ )

$$R_{mm} = \frac{\pi}{\mu_0 L \ln\left(1 + \frac{\pi g_{eff}}{\delta}\right)} \quad (9)$$

where  $g_{eff}$  is the effective airgap length and  $\delta$  is the gap between the the magnets

### 3.2. Reluctance calculation for magnet to rotor iron leakage path

The leakage reluctance of flux paths magnet to rotor iron is computed on the basis of dimensional details and their material properties using Eq. (11). Similarly, using circular arc-straight technique Fig. 8 shows the path of leakage flux between magnets to rotor iron.

Permeance of magnet to rotor iron leakage flux path ( $P_{mi}$ )

$$P_{mi} = \int_0^{g_{eff}} \frac{\mu_0 L}{H_{pm} + \pi \zeta} d\zeta = \frac{1}{R_{mi}} \quad (10)$$

Reluctance of magnet to rotor iron leakage flux path ( $R_{mi}$ )

$$R_{mi} = \frac{\pi}{\mu_0 L \ln\left(1 + \frac{\pi g_{eff}}{H_{pm}}\right)} \quad (11)$$

### 3.3. Magnetic field distribution and electromagnetic performances

The magnetic flux distribution in air gap is flat-topped due to the arc shaped magnets mounted on the rotor. This results in odd space harmonic components of the flux density. These harmonics can be reduced by proper selection of arc span of the PMs. The pole arc width is selected as 144°E which eliminates multiples of 5th order space harmonics. This short pitching of magnets reduces the weight of magnets and makes the machine cost effective.

Magnetic ux density due to PM's in the air gap

$$B_g(\theta_{er}) = \sum_{k=1,3,5}^{\infty} B_{gk} \sin(k\theta_{er}) \quad (12)$$

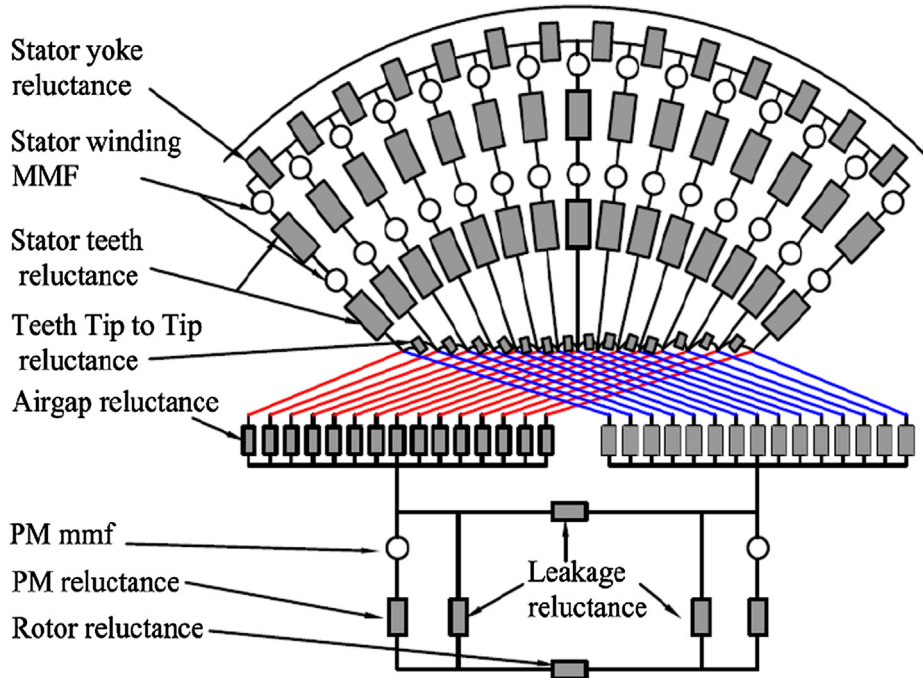


Fig. 5. DRNM of FP-PMSG.

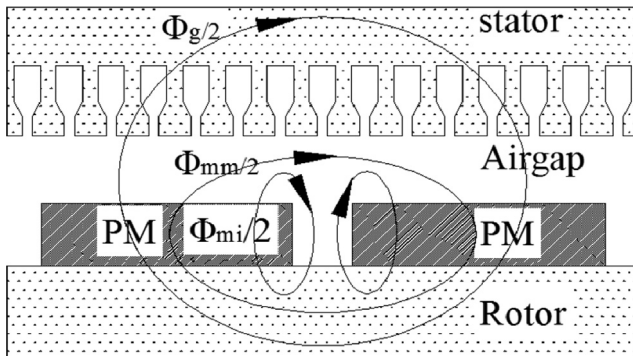


Fig. 6. Linear model.

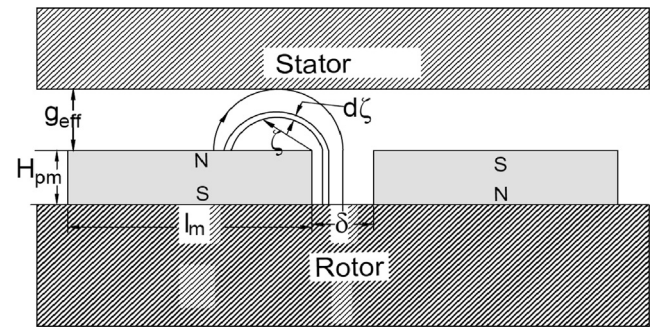


Fig. 8. Magnet to rotor iron flux path.

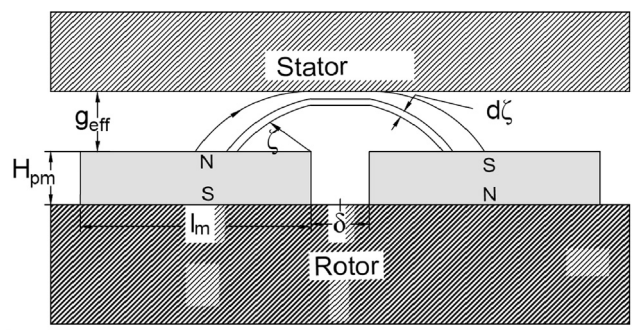


Fig. 7. Magnet to magnet flux path.

where peak value of flux density ( $B_{gk}$ ) is

$$B_{gk} = \frac{4}{\pi(\frac{\pi}{2} - \beta)} \frac{B_g}{k^2} \cos(k\beta) \sin\left(k\frac{\pi}{2}\right) \quad (13)$$

Moreover, elimination of space harmonics in the air gap flux density decreases the harmonics in the generated voltage along

with reduction in ripple torque and thereby enhances the overload capability and performance of the machine. No-load generated EMF of stator and average electromagnetic torque required the generator are represented by Eq. (14) and Eq. (17) respectively.

Generated voltage in the stator winding ( $E(t)$ )

$$E(t) = \sum_{k=1,3,7}^{\infty} E_k \sin(k\omega_e t) \quad (14)$$

where peak value of voltage ( $E_k$ ) is

$$E_k = \frac{16}{P} \times 2.9563 \times N_c L_i r_s w_e B_{gk} \cos\left(k\frac{\pi}{30}\right) \quad (15)$$

The total output power ( $P(t)$ ) is

$$P(t) = E_a(t)I_a(t) + E_b(t)I_b(t) + E_c(t)I_c(t) + E_d(t)I_d(t) + E_e(t)I_e(t) \quad (16)$$

The average electromagnetic torque ( $T(t)$ ) is

$$T(t) = (T_{cogg}) + \frac{P(t)}{\omega_e} \quad (17)$$

where  $\omega_e$  is the electrical speed of rotor.

Cogging torque ( $T_{\text{cogg}}$ ) is

$$T_{\text{cogg}} = \frac{-1}{2} \phi_g^2 \frac{d(R(\theta))}{d(\theta)} \quad (18)$$

The periodicity of cogging torque is estimated to be the least common multiple of the number of stator slots and number of rotor poles.

#### 4. Experimental setup

To test the FP-PMSG, the experimental setup was developed as shown in Fig. 9. Generator is driven by a prime-mover which fulfils the power requirement for cogging torque and the electric load. The cogging torque is an inherent behaviour of PM machine which is present throughout its operation. Machine is loaded using a five phase rectifier (FP-rectifier) circuit. The rectified direct current link

voltage is the fundamental building block for grid connected or stand alone generators, so loading of generator with the rectifier provides its actual behaviour. The no-load phase voltage and corresponding rectified output DC voltage at 26.81 Hz are 195 V and 390 V, respectively as shown in Fig. 10.

#### 5. Results and validation

The analytical results are predicted using the dynamic reluctance network method. The network consists of MMF sources along with linear, non-linear and variable reluctances. Dynamic reluctance modeling of air gap reluctance ensures the accuracy of prediction about magnetic flux distribution due to anisotropic structure of stator and rotor. Since distribution of the fluxes directly associates itself with the electromagnetic performance, so its accuracy is dependent upon its accurate prediction. The

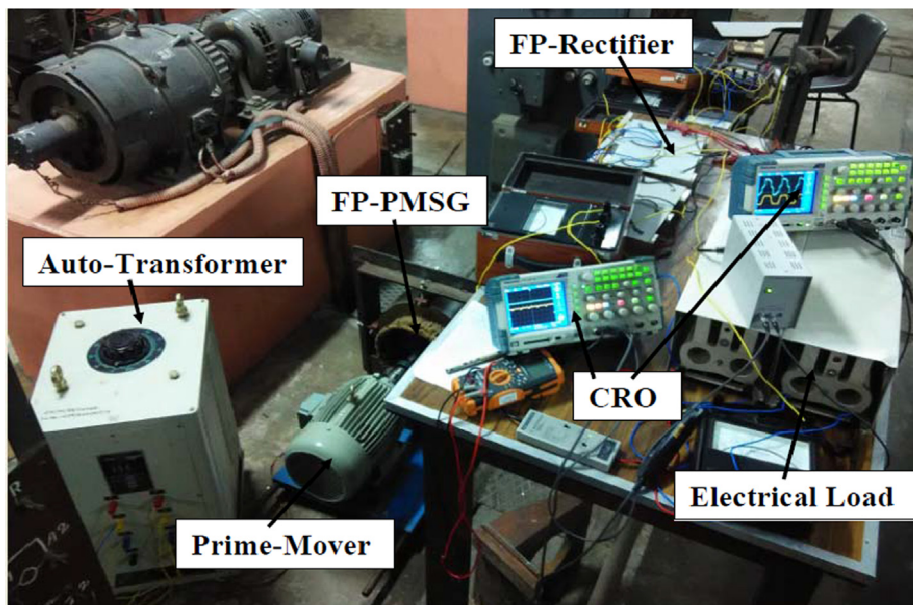


Fig. 9. Experimental set-up.

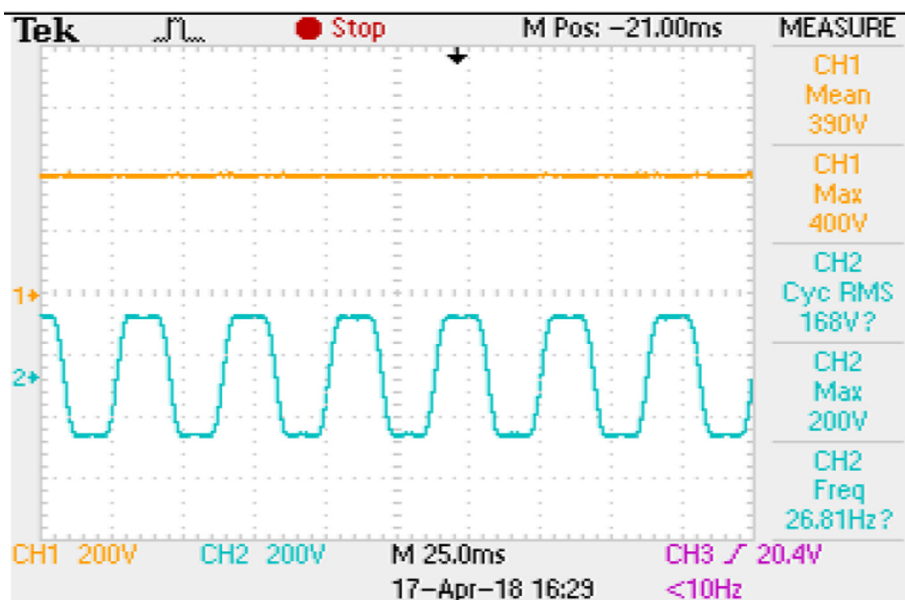


Fig. 10. DC voltage and phase voltage at 26.81 Hz.

```
STEP=1
SUB =1
TIME=1
BSUM      (AVG)
RSYS=0
SMX =1.44873
```

FEB 24 2018  
16:44:31

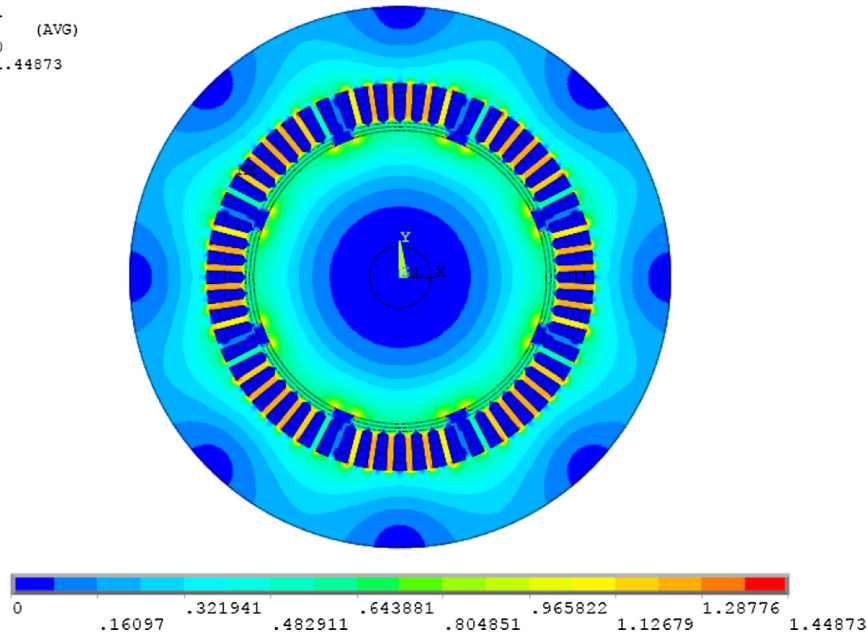


Fig. 11. Flux density.

generator performance is largely dependent upon the core saturation and its proper design goes a long way in saving the material cost and enhancing its performance. The performance analysis under loading condition of FP-PMSG is carried out using FP-rectifier. The regulation of terminal voltage of generator can be carried out by direct electrical loading of rectified DC voltage at its terminals. The analytical results are validated using FEM analysis. The Ansoft Maxwell software is used for the FEM analysis. However, the modeling is done for one fourth portion of the machine because of its quarter symmetry. The reduced model decreases the structural complexity as well as time consumption of performance analysis. In addition the no load analysis in FEM is carried out by using magnetostatic solver whereas the loading analysis is carried out by using time step transient solver. For the magnetostatic analysis, the boundary condition at all the surfaces is taken as vector potential whose value is zero. The total number of mesh elements is 1374 in triangular shape with different sizes which are generated automatically by setting of edge length for different sections in the model. The solution is converged after two passes. The profile data shows that the total real time is taken 5 s and the CPU time is taken 3 s for the convergence of the simulation. On the contrary, the transient analysis is made based on the boundary conditions which are vector potential, master and slave. The total number of mesh elements is 3142 of triangular shape with different sizes in the model. From the excitation, the generator is externally loaded together with eddy current effect is also provided by this. The time steps are set to 0.0002 s for the simulation. The profile data show that the total real time taken is 56.40 s whereas the time taken by CPU is 41.20 s for the simulation. FEM results are accurate but more time consuming compared to analytical methods. Further, these results are validated with experimental results.

### 5.1. Magnetic field distribution

Due to anisotropic structure of stator and rotor, reluctance of air gap is not fixed therefore the magnitude of flux density varies with rotor position. For the analytical prediction, 3600 rotor positions have been considered for flux density computation. Fig. 11 represents the flux density plot in the machine and is approximately

1.28 Tesla at the stator teeth and is highest at the corner of magnet-rotor interface due to leakage flux. The flux density in the air gap is evaluated using analytical and FEM analysis and is shown in Fig. 12. The predicted air gap flux density, found to be 0.5621 Tesla, is 1.282% lesser than that found using FEM. The closeness of these results reveals the effectiveness of dynamic magnetic circuit modeling.

### 5.2. Variation of EMF

The No-load generated EMF using analytical, FEM and experimental results at 400 rpm are shown in Fig. 13. The predicted result is found to be 187.56 V, which is 1.284% and 3.28% lesser than FEM and experimental results, respectively at 400 rpm.

There are two line voltages: adjacent and non-adjacent in FP-PMSG. These voltages are shown in Fig. 14 and Fig. 15. The peak value of both are same and is twice the peak value of phase voltage whereas the fundamental value of adjacent and non-adjacent line

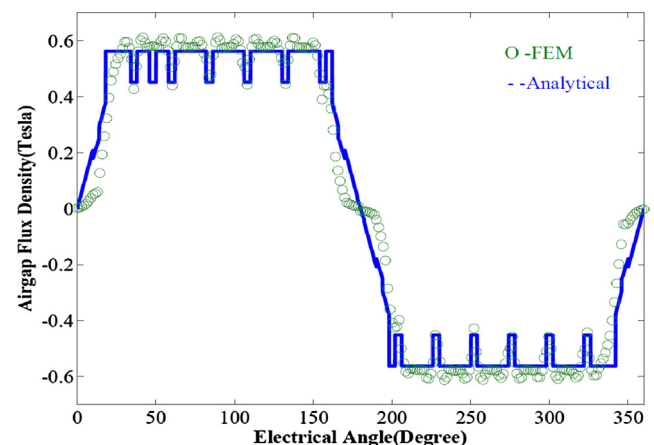


Fig. 12. FEM and analytical result of air gap flux density.

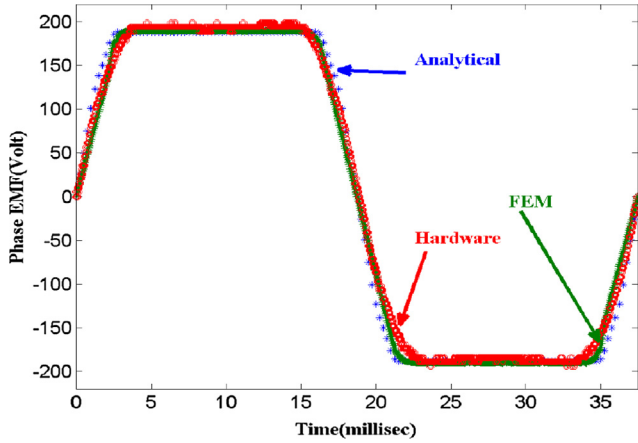


Fig. 13. Comparison of phase voltage of analytical, FEM and Hardware result.

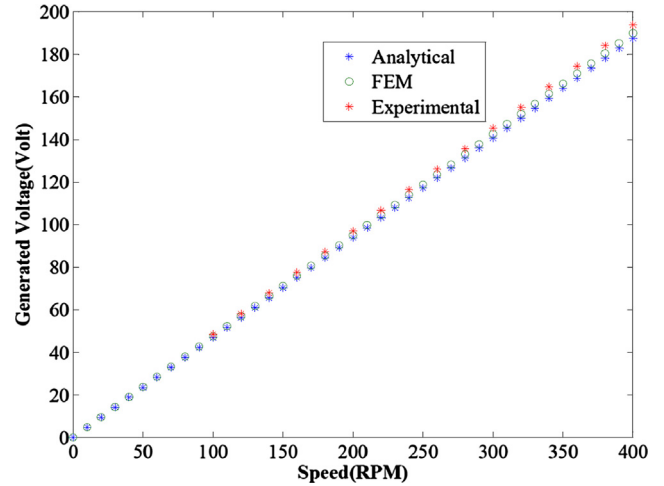


Fig. 16. Generated voltage per phase with speed.

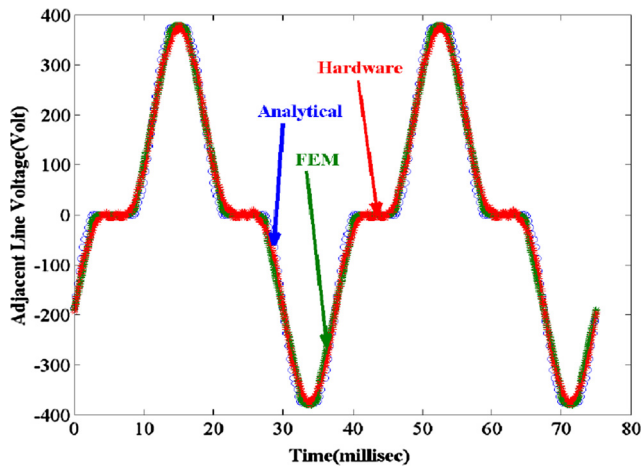


Fig. 14. Adjacent line voltage.

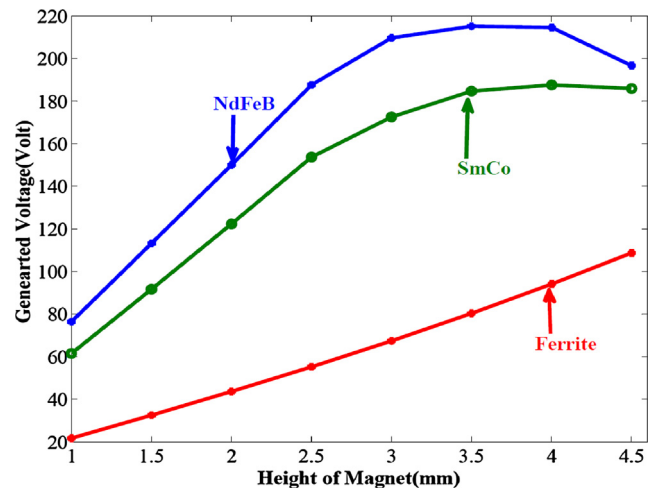


Fig. 17. Generated voltage with different grade of magnets with height of magnet.

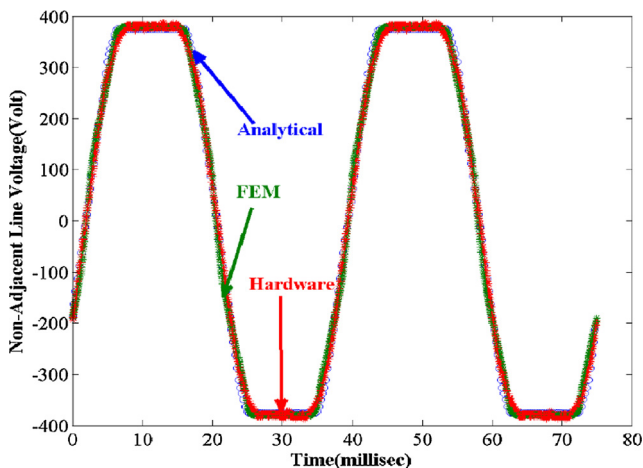


Fig. 15. Non-adjacent line voltage.

and FEM results are quite close to the experimental results. The electromagnetic performance is calculated for different PM materials like NdFeB, SmCo and ferrite. The generated voltage due to ferrite is lowest and that with NdFeB is highest because the value of  $BH_{max}$  and remanence flux density ( $B_r$ ) is least for ferrite and highest for NdFeB.

Fig. 17 represents the variation of generated voltage with the height of magnet. It is observed that the voltage due to ferrite magnet increases linearly as the height of magnet increases from 1 to 3 mm and at a slightly higher rate in between 3 and 4.5 mm because of the dominance of ferrite reluctance change over the air reluctance change in the main flux path. On the other hand, it is observed that the linear relation holds only upto 2.5 mm for NdFeB and SmCo magnets. Further, non-linearity creeps in as a consequence of saturation of stator teeth, as the height of magnet is increased from 2.5 to 3.5 mm in case of NdFeB and the maximum voltage is found to be 215.13 V at 3.5 mm. The similar non-linear behaviour is exhibited in SmCo in the range of height from 2.5 to 4 mm and maximum voltage is found to be 187.6 V at 4 mm. Further, voltage starts to decrease in range of 4–4.5 mm height of magnet and attains 196.7 and 185.9 V for NdFeB and SmCo, respectively. The analytical and FEM results for NdFeB are verified and found to be in close agreement and is shown in Fig. 18.

voltages are 1.176 and 1.902 times the fundamental value of phase voltage, respectively.

Fig. 16, represents the generated voltage-speed characteristic and the relation is found to be linear. It is found that predicted

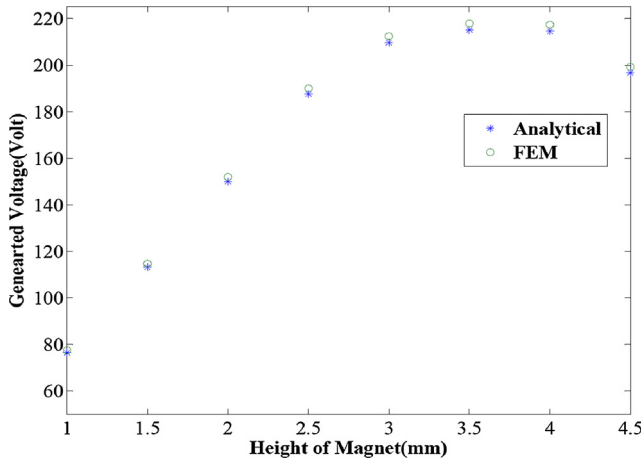


Fig. 18. Generated voltage with height of NdFeB magnet.

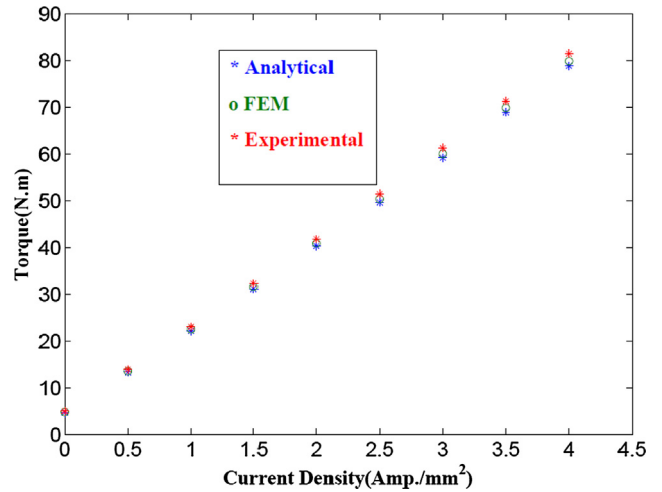


Fig. 20. Torque Vs current density.

### 5.3. Variation of torque and rectified power

The torque requirement of FP-PMSG is fulfilled by prime-mover. The torque under loaded condition comprises, average electromagnetic torque and cogging torque. Cogging torque has a negative impact during operation of machine and increases torque ripple. Fig. 19 represents an analytical and FEM variation of torque. The average torque predicted by analytical method is 78.885 N m and is 79.89 N m in case of FEM, at rated current. The percentage ripple in the torque is 9.05% and 7.4% for predicted and FEM respectively. Variation of magnitude of average torque with current density is also carried out and a linear relationship is established between the two quantities as shown in Fig. 20.

Average torque which has an initial value at zero current density, owes its existence to the cogging torque. The cogging torque is the inherent torque of PM machine and is present throughout the operation of generator and its variation is shown in Fig. 21. Its predicted result is 4.615 N m, and is 2.55% lesser than FEM. It is further validated and found 6.46% lesser than the experimental result. Generator is loaded through rectifier and variation of output DC electric power with resistive loading is carried out which is shown in Fig. 22.

### 5.4. Comparative studies between three and five phase PMSG

A comparative study between 60 slots, 8 poles, 3 phase and 60 slot, 8 pole, 5 phase PMSG is done and their performance parameters are enlisted in Table 4. For the comparison, all the dimensions,

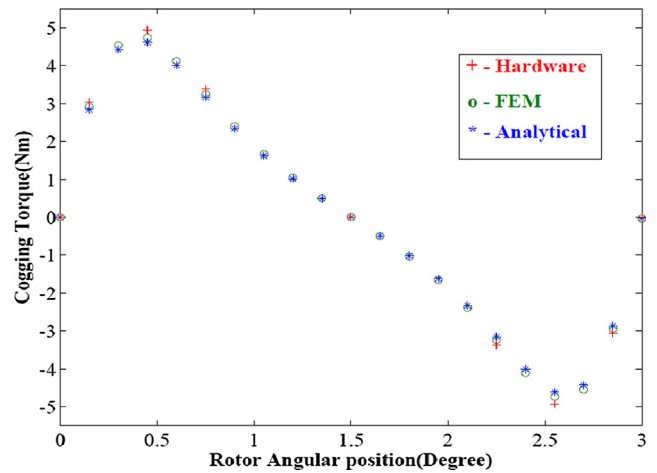


Fig. 21. Comparison of cogging Torque of analytical, FEM and Hardware result.

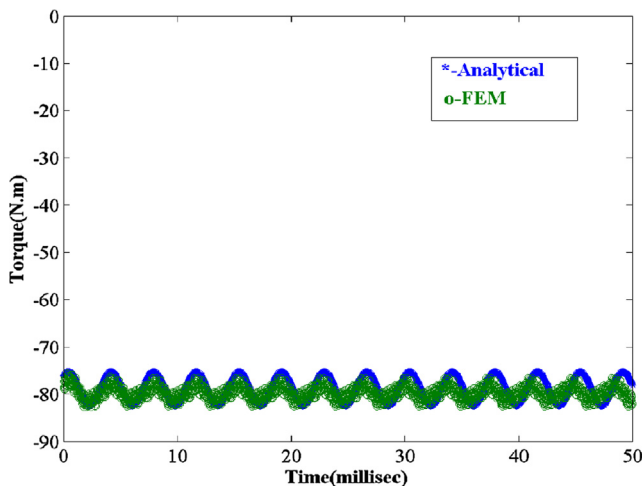


Fig. 19. Average torque.

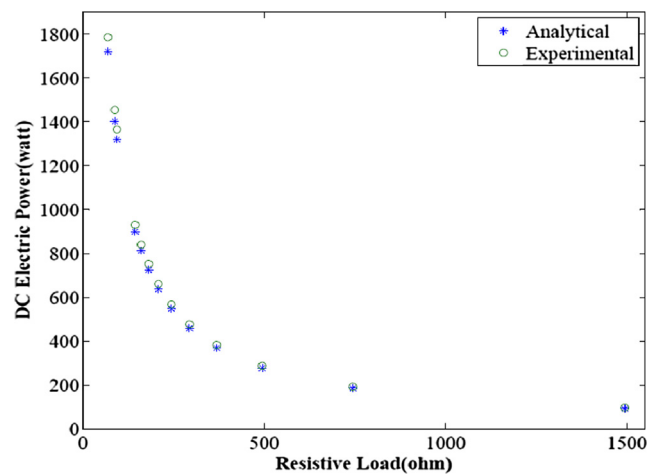
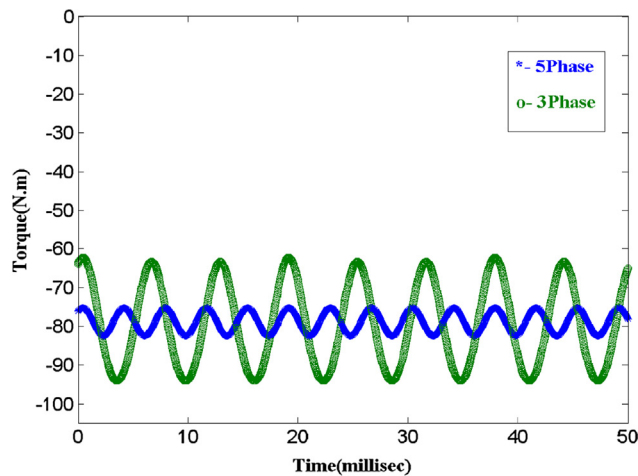


Fig. 22. Output DC Electric power with resistive load.

material properties and current rating of the generator are kept constant. It is found that the winding phase spread of five phase PMSG is lesser by 24° than three phase generator which limits the leakage flux and minimises the leakage inductance. The number of turns per phase is lesser which reduces the phase resistance that limits

**Table 4**  
Comparative performance parameters.

Parameter	5-Phase PMSG	3-Phase PMSG
Winding phase spread angle	24	48
No. Of turn per phase	456	760
Torque	78.8850	77.3909
%Ripple torque	9.05%	39.6556%
%Efficiency	92.0632	91.9002
Power to weight ratio	83.4993	81.6746



**Fig. 23.** Comparison of Torque of three phase and Five Phase PMSG.

the losses compared to three phase generator. The efficiency and power density for the five phase PMSG are found to be 92.06% and 83.499 W/kg, respectively which is higher than the conventional three phase generator. Fig. 23 presents the electromagnetic torque required for five and three phase generator and it is found that for similar torque, the percentage ripple factor is 9.05% and 39.65% respectively. Higher ripple factor shows adverse effect in terms of higher vibration and acoustic noise in the system.

## 6. Conclusion

This paper studies the design and analysis of electromagnetic behaviour of a FP-PMSG for wind power application. DRNM has been used for design and optimization of generator. The reluctance model predicted the flux distribution in the air gap and electromagnetic performance in a precise and accurate manner. In comparison with FEM, for any saturation level, predicted results are quite close to the value of generated voltage. The predicted flux density at middle of air gap and phase voltage is 0.5621 T and 187.56 V at the rated speed respectively which are 1.282% and 1.284% lesser than the obtained FEM results. Furthermore, experiment was conducted for generated phase voltage using the fabricated generator and was found to be 3.39% higher than the predicted result. Accuracy of DRNM was high as it not only considered dynamic reluctance of air gap but also considered reluctance of leakage flux paths which led to the improved design. The permeability of core material varies abruptly with saturation, thus for realisation of its adverse affect on the generated voltage, different PM materials were taken like NdFeB, SmCo and ferrite and their dimensions were varied. The generated voltage at 4.5 mm of PM thickness was found to be decreased by 8.5% and 0.9% from its peak value for NdFeB and SmCo respectively. The predicted voltage with NdFeB was in close agreement with the FEM results. In addition, the predicted electromagnetic torque was calculated under loaded conditions was 78.88 N m which was 1.25% lesser than that evaluated FEM. The ripple percentage in electromagnetic torque came out to be 9.05% and 7.4% for

predicted and FEM respectively. Hence, cogging torque was evaluated as 4.615 N m under no-load condition which was found that predicted results were 2.55% and 6.46% lesser as compared to FEM and experimental studies respectively. Generator was loaded through rectifier and the variation in electric power with resistive loading was in good agreement with experimental results. In addition, the power density and efficiency for the FP-PMSG were found to be 83.499 W/kg and 92.06%, respectively which are higher than the conventional three phase generator.

## References

- [1] Goh HH, Lee SW, Chua QS, Goh KC, Teo KTK. Wind energy assessment considering wind speed correlation in Malaysia. *Renew Sustain Energy Rev* 2016;54:1389–400.
- [2] Mahdizadeh Amin, Schmid Robert, Oetomo Denny. Enhanced energy capture of wind turbines by exact output regulation. In: IEEE 56th annual conference on decision and control (CDC), Melbourne, Australia. p. 1446–51.
- [3] Sindhuja B. A proposal for implementation of wind energy harvesting system in trains. In: International conference on control, instrumentation, energy and communication. p. 696–702.
- [4] Zhou Jiawei, Li Shengquan, Li Juan, Zhang Jin. A combined control strategy of wind energy conversion system with direct-driven PMSG. 31st Youth academic annual conference of Chinese association of automation, Wuhan, China; 2016. p. 369–74.
- [5] Aubree Rene, Auger Franois, Mace Michel, Loron Luc. Design of an efficient small wind-energy conversion system with an adaptive sensorless MPPT strategy. *Renew Energy* 2016;86:280–91.
- [6] Li H, Chen Z. Design optimization and site matching of direct-drive permanent magnet wind power generator systems. *Renew Energy* 2009;34:1175–84.
- [7] Blow Fredrik, Eriksson Sandra, Bernhoff Hans. No-load core loss prediction of PM generator at low electrical frequency. *Renew Energy* 2012;43:389–92.
- [8] Kumar Raja Ram, Singh Santosh K, Srivastava RK. Thermal modelling of dual-stator five-phase permanent magnet synchronous generator. In: IEEE transportation electrification conference (ITEC-India). p. 1–6.
- [9] Trabelsi Mohamed, Nguyen Ngac Ky, Semail Eric. Real-time switches fault diagnosis based on typical operating characteristics of five-phase permanent-magnetic synchronous machines. *IEEE Trans Ind Electron* 2016;63(8):4683–94.
- [10] Youssef Abdel-Raheem, Sayed Mahmoud A, Abdelwhab MN, Gaber Shabib. Generator side converter for five-phase PMSG based wind turbine generators using perturbation and observation technique. *Int J Power Eng Energy (IJPEE)* 2016;7(1):610–8.
- [11] Barhoumi EM, Wurtz F, Chillet C. Efficient reluctance network formulation for modeling design and optimization of linear hybrid motor. *IEEE Trans Magn* 2016;52(3). Article. 7002404.
- [12] Dalal Ankit, Nekkhalu Sameer, Kumar Praveen. 2-D analytical sub-domain model for hybrid dual-rotor motor. *IEEE Trans Magn* 2016;52(6). Article no. 8103609.
- [13] Hannon Bert, Sergeant Peter, Dupr Luc. 2-D analytical subdomain model of a slotted PMSM with shielding cylinder. *IEEE Trans Magn* 2014;50(7). Article. 8101410.
- [14] Mirahki Hooshang, Moallem Mehdi. Torque calculation in interior permanent magnet synchronous machine using improved lumped parameter models. *Prog Electromag Res M* 2014;39:133–9.
- [15] Kumar Raja Ram, Singh SK, Srivastava RK. Effect of magnetic trajectories in a magnetically coupled dual stator five phase PMSG. International conference on industrial technology (IEEE ICIT2015), Seville, Spain; 2015. p. 720–25.
- [16] Dogan H, Garbuio L, Nguyen-Xuan H, Delinchant B, Foggia A, Wurtz F. Multistatic reluctance network modeling for the design of permanent-magnet synchronous machines. *IEEE Trans Magn* 2013;49(5):2347–50.
- [17] Hanselman DC. *Brushless, permanent-magnet motor design*. New York: McGraw-Hill; 1994.



**Dr. Raja Ram Kumar** received the B. Tech. Degree in Electrical Engineering from the West Bengal University of Technology, Kolkata, India in 2010 and M. Tech. as well as Ph.D. Degree in Electrical Machines & Drives from the Indian Institute of Technology (Banaras Hindu University), Varanasi, India in 2012 and 2018, respectively. He is currently working as an Assistant Professor (Under TEQIP-III) in the Department of Electrical Engineering, Jorhat Engineering College, Assam. He received institute research award by IIT (BHU) Varanasi in 2016 and second prize paper award in IACC Annual Meeting 2018 at Portland during IAS Annual Meeting. He was the chair of student branch of IEEE-IAS at IIT (BHU) Varanasi. He is the author of several research papers which are published in international journals and conference proceedings. His current research interests include renewable energy, electrical machines, electric drives, power electronic converter design and control.



**Dr. Santosh Kumar Singh** received Ph.D. degree from the Department of Engineering, University of Cambridge (UK). He is currently an Associate Professor with the Department of Electrical Engineering, Indian Institute of Technology (BHU), Varanasi (UP) India. He is a senior member of IEEE (USA), member IEI (India) and Life member ISTE (India). He has published several research papers in international/national journals and conference proceedings. His research interests include silicon carbide converters, power electronic topologies, electric drives, and permanent magnet generators.



**Professor (Dr.) R.K. Srivastava** was born on December 06, 1960 in Mirzapur (UP) India. He received the B. Tech. Degree in Electrical Engineering, the M. Tech. Degree in Electrical Machines and Drives, and the Ph. D. Degree in Electrical Machines from the erstwhile Institute of Technology, Banaras Hindu University, Varanasi (UP) India in 1983, 1985, and 2000 respectively. He has served as teaching faculty in Pant College of Technology, Pantnagar and Institute of Engineering & Technology (IET), Lucknow (UP) India. He is currently working as a Professor in Electrical Machines and Drives in Indian Institute of Technology (Banaras Hindu University), Varanasi (UP) India. He has published several research papers in international/national journals and conference proceedings. He has authored two books. His specializations are the electromagnetic field applied to electrical machines,

electromagnetic propulsion, linear induction machines, special purpose electrical machines, permanent magnets motors and generators and Eddy current brake. He had travelled to USA, Japan and Indonesia. He is Senior Member of IEEE (USA) and an Adviser and Founder of the IEEE Industry Applications Society Student Chapter at IIT (BHU), Varanasi (India).



**Professor (Dr.) R.K. Saket** is working in the Department of Electrical Engineering at Indian Institute of Technology (Banaras Hindu University), Varanasi (UP) India. Previously, he was an Assistant Lecturer in Electrical and Electronics Engineering group at Birla Institute of Technology and Science, Pilani (Rajasthan), India; Lecturer in University Institute of Technology, Rajiv Gandhi University of Technology, Bhopal (MP), India and Assistant Professor in the Faculty of Engineering and Technology, Sam Higginbottom University of Agriculture, Technology and Sciences, Allahabad (UP), India. He has more than twenty years of teaching and research experience. He is the author/co-author of approximately 80 scientific articles, book chapters and research papers in prestigious international journals and conference proceedings. Dr. Saket is a fellow of the Institution of Engineers (India), SMIEEE (USA), MIET (UK), LMISTE (India) and an editorial board member of the Engineering, Technology and Applied Science Research (Greece). He is awarded by GYTI Award - 2018 by Hon'ble President of India at Rashtrapati Bhavan, New Delhi (India) on March 19, 2018, and Design Impact Award by Padma Vibhushan Ratan Tata at Mumbai (India) on July 24, 2018. His research interests include power system reliability, electrical machines and drives, reliability enhancement of energy systems, and renewable sources of electrical energy.